SCIENCE CHINA
Physics, Mechanics & Astronomy

• Article •

April 2023 Vol. 66 No. 4: 242011
https://doi.org/10.1007/s11433-022-2048-3

Neutron matter properties from relativistic Brueckner-Hartree-Fock theory in the full Dirac space

Xiaoying Qu[1], Hui Tong[2,3], Chencan Wang[4], and Sibo Wang[5*]

[1] *School of Mechatronics Engineering, Guizhou Minzu University, Guiyang 550025, China;*
[2] *College of Physics and Materials Science, Tianjin Normal University, Tianjin 300387, China;*
[3] *Strangeness Nuclear Physics Laboratory, RIKEN Nishina Center, Wako 351-0198, Japan;*
[4] *School of Physics and Astronomy, Sun Yat-Sen University, Zhuhai 519082, China;*
[5] *Department of Physics, Chongqing University, Chongqing 401331, China*

Received October 10, 2022; accepted November 30, 2022; published online March 3, 2023

A novel description of the strongly interacting pure neutron matter (PNM) was carried out by the relativistic Brueckner-Hartree-Fock (RBHF) theory in the full Dirac space with Bonn A potential. The scalar and vector components of the single-particle potentials are shown as functions of the momentum and the density, and are compared with the results obtained by the RBHF calculations in the Dirac space without negative-energy states. By benchmarking the binding energies of PNM to those predicted by several *ab initio* methods in the nonrelativistic framework with two- and three-body forces, we find our results are softer than those from the Brueckner-Hartree-Fock theory with the inclusion of three-body force, and in harmony with the ones obtained by the Monte Carlo method and many-body perturbation theory within uncertainties. In addition, the equation of state for neutron star matter is consistent with the constraints from multi-messenger astrophysical observation and heavy-ion collision experiments. The tidal deformabilities of a binary neutron star system are calculated and found consistent with the constraints from GW170817.

neutron matter properties, relativistic Brueckner-Hartree-Fock, full Dirac space

PACS number(s): 21.30.Fe, 21.65.+f, 26.60.+c

Citation: X. Qu, H. Tong, C. Wang, and S. Wang, Neutron matter properties from relativistic Brueckner-Hartree-Fock theory in the full Dirac space, Sci. China-Phys. Mech. Astron. **66**, 242011 (2023), https://doi.org/10.1007/s11433-022-2048-3

1 Introduction

Understanding the properties of dense neutron-rich matter is one of the frontiers in both nuclear physics and nuclear astrophysics, due to its intimate relation to the symmetry energy [1], neutron skin thickness [2, 3], and global properties of neutron stars [4]. It has been one of the most challenging topics to explore the neutron-rich matter in terms of the underlying nucleon-nucleon (*NN*) interactions. In particular, after the detection of a gravitational wave (GW) signal from a merger of a binary neutron star (BNS) system [5], the study of neutron-rich matter has entered a new era, where theoretical microscopic predictions will foreseeably be confronted with astronomical observations.

As an ideal manifestation of the extreme isospin condition for neutron-rich matter, the pure neutron matter (PNM) is of remarkable interest for a comprehensive understanding of neutron-rich nuclei and neutron stars [6]. Due to the absence of proton-neutron interactions, PNM can be easily accessible to density functional theories with effective interactions [7-11] and various *ab initio* methods starting from re-

*Corresponding author (email: sbwang@cqu.edu.cn)

alistic *NN* interactions [12-16]. In refs. [17-21], PNM is regarded as a benchmark scenario to test theoretical many-body methods and models for the *NN* interactions. By performing these benchmark calculations, the aim is not only to obtain a realistic description of PNM properties but also to quantitatively assess the systematic error of the different many-body approaches and how this error depends upon the choice of nuclear interactions.

In previous benchmark studies, nearly all the theoretical many-body methods are rooted in the nonrelativistic framework, where the three-body forces (TBFs) are indispensable for reaching satisfying descriptions of nuclear many-body systems [22]. It is well-known that, through the nucleon-antinucleon excitation, part of TBF effects can be self-consistently contained in the relativistic framework [23, 24]. Therefore, for benchmark calculation of PNM, it is of high interest to take into account the results obtained by the relativistic *ab initio* methods.

The relativistic Brueckner-Hartree-Fock (RBHF) theory [25] is one of the most important *ab initio* methods in the relativistic framework, where the single-particle motion of a nucleon in the nuclear matter is described by the Dirac equation, and the effective interaction named G matrix is derived to incorporate the two-body short-range correlations induced by the strong repulsive core.

In the RBHF calculations, one of the most important procedures is to extract self-consistently the scalar and vector components of the single-particle potentials from the G matrix [26, 27]. To avoid the complexity in the full Dirac space with both positive-energy states (PESs) and negative-energy states (NESs), the extraction is usually achieved in the Dirac space with PESs only by implementing additional approximations, e.g., the momentum-independence approximation (mom.-ind. app.) method and the projection method. The mom.-ind. app. method [28-32] assumes that the single-particle potentials are momentum independent and the spacelike part of the vector potential is negligible. The scalar potential and the timelike part of the vector potential can be extracted directly from the single-particle potential energies at two selected momenta. This method suffers from the uncertainties arising from the arbitrary choice for the reference momenta. In the projection method [33-38], the G matrix elements are projected onto a complete set of five Lorentz invariant amplitudes [33], from which the single-particle potentials are calculated. However, the choice of these Lorentz invariant amplitudes is not unique. Different schemes of projections have been used, which differ mainly due to the effects of the pseudoscalar meson exchange.

Recently, a self-consistent RBHF calculation in the full Dirac space, i.e., by considering the PESs and NESs simultaneously, has been achieved for symmetric nuclear matter (SNM) [39, 40] and asymmetric nuclear matter (ANM) [41, 42]. By decomposing the matrix elements of the single-particle potential operator in the full Dirac space, the momentum dependent scalar and vector components of the single-particle potentials are determined uniquely. The long-standing controversy about the isospin dependence of the effective Dirac mass in relativistic *ab initio* calculations of ANM is also clarified [41].

In this work, the RBHF theory in the full Dirac space is applied to describe the properties of PNM. The importance of the completeness of the Dirac space can be demonstrated by comparing our results to those obtained by the mom.-ind. app. method and the projection method. After showing the scalar and vector components of the single-particle potentials as functions of the momentum and the density, we move to the binding energies of PNM, which will be benchmarked to those obtained by various nonrelativistic *ab initio* methods. In addition, the predictions on the equation of state (EOS) for neutron star matter and the global properties of neutron stars will be compared to the recent constraints from astronomical observations.

This paper is organized as follows. In sect. 2, the theoretical framework of the RBHF theory in the full Dirac space is introduced. The calculated results and discussions are presented in sect. 3. Finally, a summary is given in sect. 4.

2 Theoretical framework

RBHF theory is the relativistic extension of the Brueckner-Hartree-Fock (BHF) theory, which represents the lowest order within the Bethe-Brueckner-Goldstone (BBG) expansion [26, 27]. In the RBHF theory, the single-particle motion of a nucleon in the nuclear matter is described by the Dirac equation

$$(\boldsymbol{\alpha}\cdot\mathbf{p}+\beta M+\beta\mathcal{U})u(\mathbf{p},s)=E_{\mathbf{p}}u(\mathbf{p},s), \tag{1}$$

where $\boldsymbol{\alpha}$ and β are the Dirac matrices, M is the rest mass of the nucleon, and u is the positive-energy spinor with momentum $\mathbf{p}$, single-particle energy $E_{\mathbf{p}}$ and spin s. The medium effects are manifested by the single-particle potential (operator) $\mathcal{U}$. Due to the limitation of the symmetries, the operator $\mathcal{U}$ has the general form [43]

$$\mathcal{U}(\mathbf{p})=U_{\mathrm{S}}(p)+\gamma^0U_0(p)+\boldsymbol{\gamma}\cdot\hat{\mathbf{p}}U_{\mathrm{V}}(p). \tag{2}$$

The quantities $U_{\mathrm{S}}(p)$, $U_0(p)$, and $U_{\mathrm{V}}(p)$ are the scalar potential, timelike part, and spacelike part of the vector potential, respectively. $\hat{\mathbf{p}}=\mathbf{p}/|\mathbf{p}|$ denotes the unit vector parallel to the momentum $\mathbf{p}$. By virtue of the following effective quantities:

$$\mathbf{p}^*=\mathbf{p}+\hat{\mathbf{p}}U_{\mathrm{V}}(p), \tag{3}$$

$$M^*_{\mathbf{p}}=M+U_{\mathrm{S}}(p), \tag{4}$$

$$E^*_{\mathbf{p}} = E_{\mathbf{p}} - U_0(p), \tag{5}$$

the Dirac equation (1) in the nuclear medium can be rewritten as:

$$\left(\boldsymbol{\alpha}\cdot\mathbf{p}^* + \beta M^*_{\mathbf{p}}\right) u(\mathbf{p},s) = E^*_{\mathbf{p}} u(\mathbf{p},s), \tag{6}$$

where $E^*_{\mathbf{p}} = \sqrt{M^{*2}_{\mathbf{p}} + \mathbf{p}^{*2}}$. The positive-energy spinor u and negative-energy spinor v are obtained as:

$$u(\mathbf{p},s) = \sqrt{\frac{E^*_{\mathbf{p}} + M^*_{\mathbf{p}}}{2M^*_{\mathbf{p}}}} \begin{bmatrix} 1 \\ \frac{\boldsymbol{\sigma}\cdot\mathbf{p}^*}{E^*_{\mathbf{p}} + M^*_{\mathbf{p}}} \end{bmatrix} \chi_s, \tag{7a}$$

$$v(\mathbf{p},s) = \gamma^5 u(\mathbf{p},s) = \sqrt{\frac{E^*_{\mathbf{p}} + M^*_{\mathbf{p}}}{2M^*_{\mathbf{p}}}} \begin{bmatrix} \frac{\boldsymbol{\sigma}\cdot\mathbf{p}^*}{E^*_{\mathbf{p}} + M^*_{\mathbf{p}}} \\ 1 \end{bmatrix} \chi_s, \tag{7b}$$

where χ_s is the spin wave function. The positive-energy spinor u and negative-energy spinor v form a complete basis in the Dirac space.

The Dirac equation (1) can be solved exactly once the single-particle potentials are determined. To achieve this, three matrix elements of $\mathcal{U}(\mathbf{p})$ in the full Dirac space are introduced as in refs. [44, 45],

$$\begin{aligned}\Sigma^{++}(p) &= \bar{u}(\mathbf{p},1/2)\mathcal{U}(\mathbf{p})u(\mathbf{p},1/2) \\ &= U_S(p) + \frac{E^*_{\mathbf{p}}}{M^*_{\mathbf{p}}}U_0(p) + \frac{p^*}{M^*_{\mathbf{p}}}U_V(p),\end{aligned} \tag{8a}$$

$$\begin{aligned}\Sigma^{-+}(p) &= \bar{v}(\mathbf{p},1/2)\mathcal{U}(\mathbf{p})u(\mathbf{p},1/2) \\ &= \frac{p^*}{M^*_{\mathbf{p}}}U_0(p) + \frac{E^*_{\mathbf{p}}}{M^*_{\mathbf{p}}}U_V(p),\end{aligned} \tag{8b}$$

$$\begin{aligned}\Sigma^{--}(p) &= \bar{v}(\mathbf{p},1/2)\mathcal{U}(\mathbf{p})v(\mathbf{p},1/2) \\ &= -U_S(p) + \frac{E^*_{\mathbf{p}}}{M^*_{\mathbf{p}}}U_0(p) + \frac{p^*}{M^*_{\mathbf{p}}}U_V(p),\end{aligned} \tag{8c}$$

where the direction of $\mathbf{p}$ is taken along the z-axis.

Once $\Sigma^{++}(p)$, $\Sigma^{-+}(p)$, and $\Sigma^{--}(p)$ are obtained, single-particle potentials in eq. (2) can be determined uniquely through

$$U_S(p) = \frac{\Sigma^{++}(p) - \Sigma^{--}(p)}{2}, \tag{9a}$$

$$U_0(p) = \frac{E^*_{\mathbf{p}}}{M^*_{\mathbf{p}}}\frac{\Sigma^{++}(p) + \Sigma^{--}(p)}{2} - \frac{p^*}{M^*_{\mathbf{p}}}\Sigma^{-+}(p), \tag{9b}$$

$$U_V(p) = -\frac{p^*}{M^*_{\mathbf{p}}}\frac{\Sigma^{++}(p) + \Sigma^{--}(p)}{2} + \frac{E^*_{\mathbf{p}}}{M^*_{\mathbf{p}}}\Sigma^{-+}(p). \tag{9c}$$

This effectively avoids the approximations usually adopted in the Dirac space with PESs only. Matrix elements $\Sigma^{++}(p)$, $\Sigma^{-+}(p)$, and $\Sigma^{--}(p)$ can be calculated alternatively by summing up the effective two-body interaction G matrix with all the nucleons inside the Fermi sea in the Hartree-Fock approximation:

$$\begin{aligned}\Sigma^{++}(p) = \sum_{s'}\int_0^{k_F}\frac{\mathrm{d}^3p'}{(2\pi)^3}\frac{M^*_{\mathbf{p}'}}{E^*_{\mathbf{p}'}} \\ \cdot\langle\bar{u}(\mathbf{p},1/2)\bar{u}(\mathbf{p}',s')|\bar{G}^{++++}(W)|u(\mathbf{p},1/2)u(\mathbf{p}',s')\rangle,\end{aligned} \tag{10a}$$

$$\begin{aligned}\Sigma^{-+}(p) = \sum_{s'}\int_0^{k_F}\frac{\mathrm{d}^3p'}{(2\pi)^3}\frac{M^*_{\mathbf{p}'}}{E^*_{\mathbf{p}'}} \\ \cdot\langle\bar{v}(\mathbf{p},1/2)\bar{u}(\mathbf{p}',s')|\bar{G}^{-+++}(W)|u(\mathbf{p},1/2)u(\mathbf{p}',s')\rangle,\end{aligned} \tag{10b}$$

$$\begin{aligned}\Sigma^{--}(p) = \sum_{s'}\int_0^{k_F}\frac{\mathrm{d}^3p'}{(2\pi)^3}\frac{M^*_{\mathbf{p}'}}{E^*_{\mathbf{p}'}} \\ \cdot\langle\bar{v}(\mathbf{p},1/2)\bar{u}(\mathbf{p}',s')|\bar{G}^{-+-+}(W)|v(\mathbf{p},1/2)u(\mathbf{p}',s')\rangle.\end{aligned} \tag{10c}$$

The Fermi momentum is denoted by k_F, which is related to the total baryon number density via $\rho = k_F^3/(3\pi^2)$ for PNM. The antisymmetrized G matrix is expressed with $\bar{G}$, where the $\pm$ signs in the superscript denote the PESs or NESs. W is the starting energy, whose schemes in the full Dirac space are referred to ref. [39].

The effective interaction G matrix is the solution of in-medium Thompson equation [46], which describes the scattering of two nucleons in the nuclear matter in a relativistic framework. In the rest frame of nuclear matter, the Thompson equation reads [28]

$$\begin{aligned}G(\mathbf{q}',\mathbf{q}|\mathbf{P},W) = V(\mathbf{q}',\mathbf{q}|\mathbf{P}) + \int\frac{\mathrm{d}^3k}{(2\pi)^3}V(\mathbf{q}',\mathbf{k}|\mathbf{P}) \\ \cdot\frac{M^*_{\mathbf{P}+\mathbf{k}}M^*_{\mathbf{P}-\mathbf{k}}}{E^*_{\mathbf{P}+\mathbf{k}}E^*_{\mathbf{P}-\mathbf{k}}}\frac{Q(\mathbf{k},\mathbf{P})}{W - E_{\mathbf{P}+\mathbf{k}} - E_{\mathbf{P}-\mathbf{k}}}G(\mathbf{k},\mathbf{q}|\mathbf{P},W).\end{aligned} \tag{11}$$

The labels of PESs and NESs have been suppressed. The center-of-mass and relative momenta of the two interacting particles with momenta $\mathbf{k}_1$ and $\mathbf{k}_2$ are denoted with $\mathbf{P} = \frac{1}{2}(\mathbf{k}_1 + \mathbf{k}_2)$ and $\mathbf{k} = \frac{1}{2}(\mathbf{k}_1 - \mathbf{k}_2)$. The initial, intermediate, and final relative momenta of the two nucleons scattering in the nuclear matter are denoted by $\mathbf{q}$, $\mathbf{k}$, and $\mathbf{q}'$, respectively. The NN scattering in the nuclear medium is restricted with the Pauli operator $Q(\mathbf{k},\mathbf{P})$, which prohibits the scattering to occupied states.

Eqs. (1), (9)-(11) constitute a coupled system that has to be solved in a self-consistent way. In BBG expansion formalism, the ground-state energy of infinite nuclear matter is computed from a diagrammatic expansion, which is regrouped according to the number of independent hole lines. Within the (R)BHF approach, the energy is given by the sum of only two-hole-line diagrams, including the effect of two-body correlations through the in-medium two-body scattering G matrix:

$$E/A = \frac{1}{\rho}\sum_s\int_0^{k_F}\frac{\mathrm{d}^3p}{(2\pi)^3}\frac{M^*_{\mathbf{p}}}{E^*_{\mathbf{p}}}\langle\bar{u}(\mathbf{p},s)|\boldsymbol{\gamma}\cdot\mathbf{p} + M|u(\mathbf{p},s)\rangle - M$$

$$+\frac{1}{2\rho}\sum_{s,s'}\int_0^{k_\mathrm{F}}\frac{\mathrm{d}^3p}{(2\pi)^3}\int_0^{k_\mathrm{F}}\frac{\mathrm{d}^3p'}{(2\pi)^3}\frac{M^*_{\mathbf{p}}}{E^*_{\mathbf{p}}}\frac{M^*_{\mathbf{p}'}}{E^*_{\mathbf{p}'}}$$
$$\cdot\langle\bar{u}(\mathbf{p},s)\bar{u}(\mathbf{p}',s')|\bar{G}^{++++}(W)|u(\mathbf{p},s)u(\mathbf{p}',s')\rangle, \quad (12)$$

where the starting energy is chosen as $W = E_{\mathbf{p}} + E_{\mathbf{p}'}$.

3 Results and discussion

Relativistic *NN* interaction constitutes the basic input quantity for the RBHF theory. Combining the high-precision relativistic chiral *NN* interaction [47] will play an important role in the near future, but it is still difficult to achieve up to now. At present, the One-Boson-Exchange-Potential (OBEP) [48] is still the most economical and quantitative phenomenology for describing the *NN* interaction. The RBHF theory can describe satisfactorily the saturation properties for SNM based on OBEP [28, 36, 39]. Therefore, the relativistic *NN* interaction, i.e., the Bonn A potential, is used in the present work.

Starting from the realistic *NN* interaction Bonn A [48], the RBHF calculations for PNM are performed in the full Dirac space. One of the essential quantities in the RBHF calculation are the single-particle potentials, which are determined self-consistently by an iterative procedure. In Figure 1, the single-particle potentials U_S, U_0, and U_V at density $\rho = 0.16$ fm^{-3} are shown with red solid lines as functions of the momentum p. From zero momentum to the Fermi momentum, the relative variations for $U_\mathrm{S}(p)$ and $U_0(p)$ are approximately 4.2% and 6.7%, exhibiting a weak momentum dependence. The magnitude for the spacelike part of the vector potential U_V is apparently smaller than that of U_S and U_0. These two features are similar to the case for SNM in ref. [39]. Furthermore, we also show the results obtained in the Dirac space with PESs only in Figure 1, where the projection method with the *ps* representation for the subtracted T matrix [37] and the mom.-ind. app. method [28] are used. In comparison with the results obtained in the full Dirac space, the projection method leads to a qualitatively consistent momentum dependence with less pronounced amplitudes of U_S and U_0. This indicates that the approximation schemes and techniques used in the projection method are reliable to determine the Lorentz and isovector structure of the single-particle potentials to some extent. As for the mom.-ind. app. method, it has been shown that this method is relatively reliable in SNM [39]. However, obvious deviations are found for the mom.-ind. app. method when extended to study PNM. To obtain the uncertainties of single-particle potentials introduced by the mom.-ind. app. method, U_V is neglected, and U_S and U_0 are assumed to be momentum independent and are extracted from the single-particle potential energies at two different momenta k_1, k_2. By varying one momentum k_1 from $0.1k_\mathrm{F}$ to $0.9k_\mathrm{F}$ and the other one k_2 from $0.2k_\mathrm{F}$ to $1.0k_\mathrm{F}$ in steps of $0.1k_\mathrm{F}$, the uncertainties are shown schematically by the shaded regions in Figure 1. Considerable uncertainties of about 50 MeV are found for both potentials U_S and U_0. The deviations of the mom.-ind. app. method are not unexpected since it has been found that this method fails to determine the correct behavior of the isospin dependence of the single-particle potentials [49, 50]. Taking the advantage of the full Dirac space, the underlying reason for the failure of the mom.-ind. app. method in ANM can be studied from a new perspective in future work.

In Figure 2, the single-particle potentials U_S, U_0, and U_V

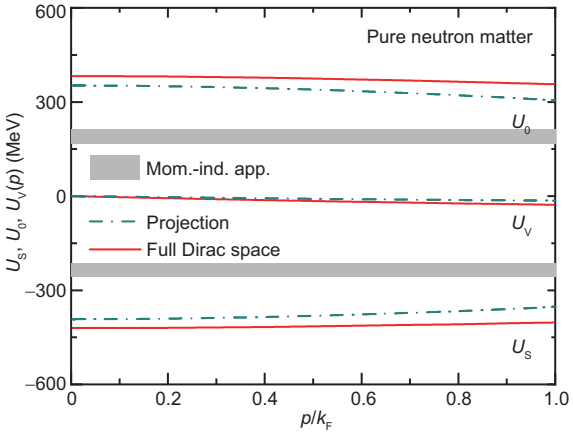

Figure 1 (Color online) Momentum dependence of the single-particle potentials U_S, U_0, and U_V for PNM calculated by the RBHF theory in the full Dirac space (red solid line) using the potential Bonn A [48], in comparison with the results obtained with the projection method (cyan dash-dotted line) and the mom.-ind. app. method (gray regions). The total baryon number density ρ is chosen as 0.16 fm^{-3} ($k_\mathrm{F} \approx 1.69$ fm^{-1}).

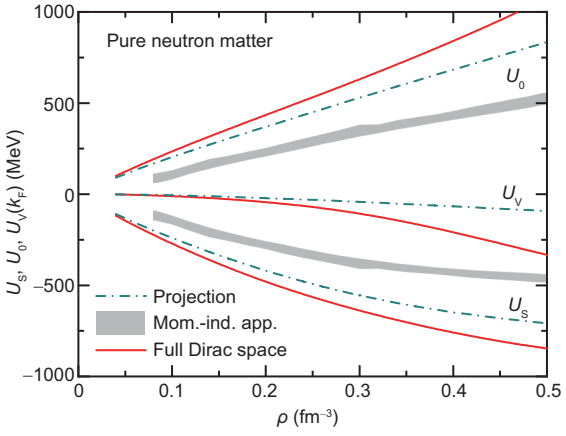

Figure 2 (Color online) Density dependence of the single-particle potentials U_S, U_0, and U_V at the Fermi momentum for PNM calculated by the RBHF theory in the full Dirac space (red solid line) using the potential Bonn A [48], in comparison with the results obtained with the projection method (cyan dash-dotted line) and the mom.-ind. app. method (gray regions).

at the Fermi momentum obtained in the full Dirac space are shown with red solid lines as functions of the density ρ. It can be seen that both U_S and U_0 are strongly density dependent. With the increase of the density, the timelike part of the vector potential U_0 shows a linearly increasing tendency, while weak saturation is found for the scalar potential U_S at higher density. The difference between the density dependence of U_S and U_0 is crucial for the saturation of the SNM in the relativistic framework [51]. It is noticeable that the spacelike part of the vector potential U_V decreases rapidly for the density higher than 0.3 fm^{-3}. This implies that it is necessary to consider U_V at high density. For comparison, the results obtained by the projection method and mom.-ind. app. method are also shown in Figure 2. It is also found that, the projection method leads to a qualitatively consistent density dependence, and the differences become more and more evident with the increasing density. The uncertainties obtained with the mom.-ind. app. method are depicted by shaded regions, which share no overlap with the other two methods.

In Figure 3, the binding energies per particle E/A for PNM calculated by the RBHF theory in the full Dirac space with Bonn A are depicted with the red solid line. The results with Bonn B and C are almost identical to the ones with Bonn A and are not shown. This is reasonable since the main difference among Bonn A, B, and C is in the tensor force strength, which is mostly reflected in the $(T = 0)$ $^3S_1$-$^3D_1$ states. In PNM, this partial wave does not contribute to the $(T = 1)$ neutron-neutron state [52]. Figure 3 also shows the binding energies obtained in the Dirac space with PESs only by using

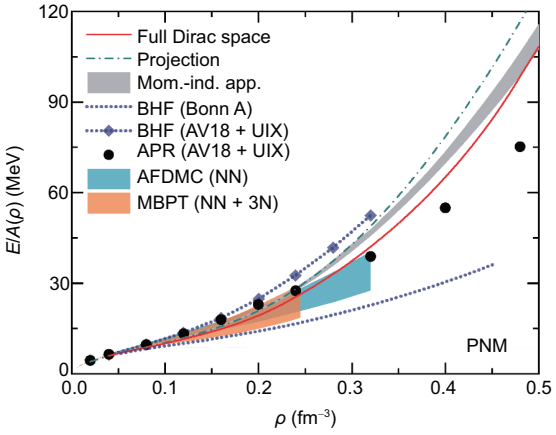

Figure 3 (Color online) The binding energy per particle E/A for PNM as a function of the density ρ calculated by the RBHF theory in the full Dirac space (red solid line), in comparison with the results obtained by the projection method (cyan dash-dotted line) and the mom.-ind. app. method (gray regions). The results obtained with other nonrelativistic *ab initio* methods are also shown, including the BHF theory with [21] or without 3*N* force [52], the variational method with AV18 and UIX [12] labeled as APR, and the AFDMC method [53] and the MBPT [54] using the chiral *NN* + 3*N* forces.

the projection method and the mom.-ind. app. method. The E/A obtained by the projection method is larger than that by the RBHF theory in the full Dirac space, and the deviation becomes more evident at higher density. With the increase of the density, the uncertainties of binding energies obtained by the mom.-ind. app. method are gradually increased. Moreover, the binding energies obtained by the mom.-ind. app. method are softer than those of the projection method, but stiffer than the prediction of the RBHF theory in the full Dirac space. Thus, the differences among the three methods confirm essentially the importance of the completeness of the Dirac space.

To understand the predicted binding energies per particle in a more comprehensive way, we compare our results with those obtained in the nonrelativistic *ab initio* methods, including the BHF theory with [21] or without three-nucleon (3*N*) force [52], the variational method (labeled as APR) [12], the auxiliary-field diffusion Monte Carlo (AFDMC) method [53], and the many-body perturbation theory (MBPT) [54]. For BHF with 3*N* force and APR, the Argonne v_{18} (AV18) *NN* interaction combined with the Urbana-IX (UIX) TBF is used. The local interactions derived from chiral effective field theory (EFT) up to next-to-next-to-leading order (N^{2}LO) are employed in the AFDMC simulations, while the chiral *NN* force up to next-to-next-to-next-to-leading order (N^{3}LO) and 3*N* force up to N^{2}LO are used in the MBPT calculations up to third-order. The increasing deviations with density between the RBHF and BHF theories by using the same realistic *NN* interaction have manifested the repulsive relativistic effect in PNM, which is consistent with those results found in SNM [30, 52]. This can be understood by the fact that, through virtual nucleon-antinucleon excitations in the intermediate states (the so-called *Z* diagram), relativistic effects lead to part of the 3*N* forces [23]. It is clear that the binding energies calculated with the BHF theory with 3*N* force are much more repulsive than those obtained by the RBHF theory in the full Dirac space. For density below about 0.3 fm^{-3}, our results are close to the ones of APR, while for higher density, the differences become evident. The uncertainties of the predictions from AFDMC method and MBPT are shown with shaded regions. For AFDMC, the uncertainties of many-body calculations include both the statistical Monte Carlo errors and the uncertainties coming from the truncation of the chiral expansion. For MBPT, the uncertainties include the errors arising from the convergence in many-body perturbation theory, missing terms in the chiral expansion, and choices of momentum-space cutoffs ($\Lambda \sim$ 400-500 MeV). It is found that the binding energies of PNM calculated with the AFDMC method and the MBPT are in harmony with our results within the uncertainties.

In principle, one would like to carry out a comparison between many-body approaches by starting from the same underlying *NN* interactions and TBF. Nevertheless, due to the complexity of *ab initio* methods and the realistic *NN* interactions, such a comparison is not applicable yet. For example, nonlocal potentials are not amenable in Monte Carlo simulations and the relativistic *NN* interactions are rather rare [47]. Considering that these underlying *NN* interactions, though different, can describe the *NN* scattering phase shifts and deuteron properties fairly well, the comparison between many-body approaches is still meaningful.

Since the neutron-rich matter dominates in the neutron star interiors, the properties of PNM are crucial for the prediction of the EOS for neutron star matter. The theoretical EOS of neutron matter is often used to study of the properties of neutron stars [52]. Starting from the binding energies of PNM and SNM, the EOS for neutron star matter, i.e., the relations among the pressure, energy density, and baryon number density, can be constructed by considering the chemical equilibrium [52]. The neutron star matter here is assumed to be composed of nucleons and leptons without considering the onset of phase transition above the saturation density. In the past few years, the observation of GW signal from a merger of a BNS system GW170817 [55] together with the followed observation of the associated electromagnetic emissions [56-58], has opened a significant multimessenger era in the field of astrophysics and nuclear physics. In particular, the GW signal provides significant constraints on the EOS of dense matter [5, 59]. In the upper panel of Figure 4, the pressure P for neutron star matter as a function of the energy density ε calculated by the RBHF theory in the full Dirac space, the projection method, and the mom.-ind. app. method is displayed. For clarity, the two momenta in the RBHF calculation with the mom.-ind. app. method are fixed as $0.7k_{\rm F}$ and $1.0k_{\rm F}$. In comparison, the pressure obtained in ref. [5] by using the spectral EOS parametrization as well as GW170817 data and imposing a lower limit on the maximum neutron star mass being $1.97M_{\odot}$ [60] is also shown. The dark (light) shaded region corresponds to the 50% (90%) posterior credible level and the purple dashed lines show the 90% prior credible interval. It is found that the EOS from RBHF theory is consistent with the constraints from GW170817. By using the RBHF theory in the full Dirac space, the pressure at twice (six times) the nuclear saturation density $\rho_0 = 0.16$ fm^{-3} is predicted to be 3.09×10^{34} (9.51×10^{35}) dyn/cm^2, which lies in the range $3.5^{+2.7}_{-1.7}\times10^{34}$ ($9.0^{+7.9}_{-2.6}\times10^{35}$) dyn/cm^2 at the 90% level in Figure 4.

Complementary to astrophysical observations, the terrestrial heavy-ion collision (HIC) experiments can also probe the properties of dense matter. In ref. [61], the HIC data of gold nuclei at relativistic energies are combined with the data

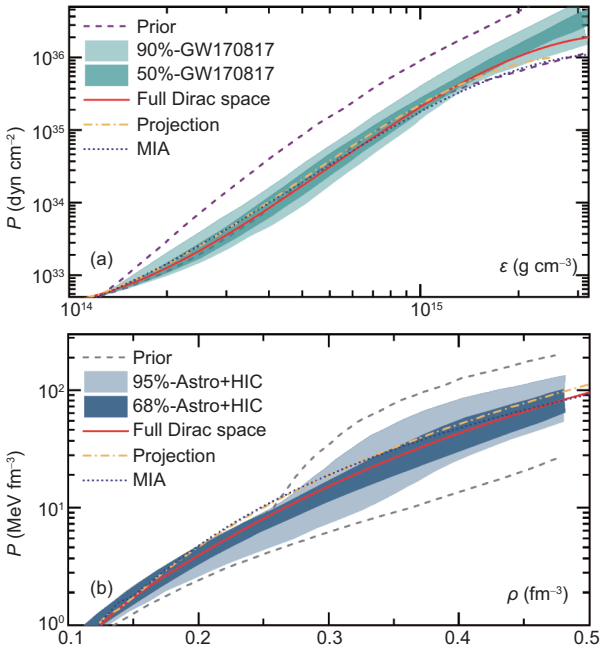

Figure 4 (Color online) (a) The pressure P for neutron star matter as a function of energy density ε calculated by the RBHF theory in the full Dirac space (red solid line), in comparison with the projection method (orange dash-dotted line), the mom.-ind. app. method (labeled as MIA, blue dotted line) and the constraints obtained by using the spectral EOS parametrization and imposing a lower limit on the maximum neutron star mass being $1.97M_{\odot}$ [5]. (b) The pressure P for neutron star matter as a function of baryon number density ρ calculated by the RBHF theory in the full Dirac space (red solid line), in comparison with the projection method (orange dash-dotted line), the mom.-ind. app. method (labeled as MIA, blue dotted line), and the constraints obtained by combining both the data from multi-messenger neutron-star observations and HIC data [61].

from astrophysical multi-messenger observations of neutron stars and microscopic nuclear theory calculations with Bayesian inference. The final constraints are shown in the lower panel of Figure 4, where the dark (light) shaded region corresponds to the 95% (68%) credible interval. Remarkable consistency is also found between the pressure predicted with the RBHF theory in the full Dirac space and the joint constraints. These comparisons in Figure 4 support firmly the applications of the RBHF theory in the full Dirac space to neutron stars in our previous works [41, 42, 62]. In addition, around the density $\rho = 0.25$ fm^{-3}, one can note that only the pressure predicted by the RBHF theory in the full Dirac space can situate inside the 68% and 95% probability contours and they are smaller than those obtained from the projection method and the mom.-ind. app. method. Therefore, the RBHF calculations in the full Dirac space predict the softest EOS, which would be more favored by the astrophysical observations and the terrestrial HIC experiments.

Based on the EOS for neutron star matter from the RBHF theory, the neutron star mass, radius, and tidal deformability can be calculated. The maximum mass of neutron stars

predicted from the RBHF theory in the full Dirac space is $2.43M_\odot$ [41]. Therefore, the EOS from the RBHF theory in the full Dirac space is stiff enough to be consistent with the observed lower bound on the maximum mass of neutron stars for $M_{\max} > 2M_\odot$ [60, 63-66]. The radius $R_{1.4M_\odot}$ of a neutron star with mass $M = 1.4M_\odot$ is 11.97 km, which is consistent with other works, such as $R_{1.4M_\odot} \leqslant 13.76$ km [67], $R_{1.4M_\odot} \leqslant 13.6$ km [59], and 9.0 km $\leqslant R_{1.4M_\odot} \leqslant 13.6$ km [68, 69] obtained from the tidal deformability [55, 70]. In the context of GW170817, the relation between the tidal deformabilities Λ_1 and Λ_2 of the BNS system can be obtained from the chirp mass $\mathcal{M} = (M_1M_2)^{3/5}(M_1 + M_2)^{-1/5} = 1.188M_\odot$, which are shown in Figure 5. As a comparison, the 50% and 90% probability contours recommended by the LIGO and Virgo observatories with the low-spin priors are also plotted [5]. It can be seen that the three curves predicted by the RBHF theory are all located on the left side of the 90% contour. In addition, one can see that the tidal deformabilities from the RBHF theory in the full Dirac space are significantly lower than those from the projection method and the mom.-ind. app. method. It indicates that the RBHF theory in the full Dirac space predicts the softest EOS, as previously shown in Figure 4.

4 Summary

Starting from the realistic nucleon-nucleon Bonn A potential, the RBHF theory is applied to PNM. The scalar and vector components of the single-particle potentials are extracted uniquely in the full Dirac space and compared with the results obtained with the projection method and the momentum-independence approximation method. The momentum dependence of the single-particle potentials is much weak, while the density dependence is strong. By benchmarking the binding energies per particle of PNM to those obtained with several popular *ab initio* methods in the nonrelativistic framework, we find our results are softer than the Brueckner-Hartree-Fock ones with the inclusion of three-body force, and in harmony with the Monte Carlo results and many-body perturbation theory within uncertainties. Our calculations provide a novel description of the strongly interacting PNM besides the nonrelativistic framework in the literature. In addition, the EOS for neutron star matter is established by combing the binding energies of PNM and symmetric nuclear matter. The EOS is found to be consistent with the constraints from astrophysical observations as well as heavy-ion collisions. The relation between the tidal deformabilities Λ_1 and Λ_2 of the binary neutron star system is located on the left side of the 90% contour which are favored by GW170817.

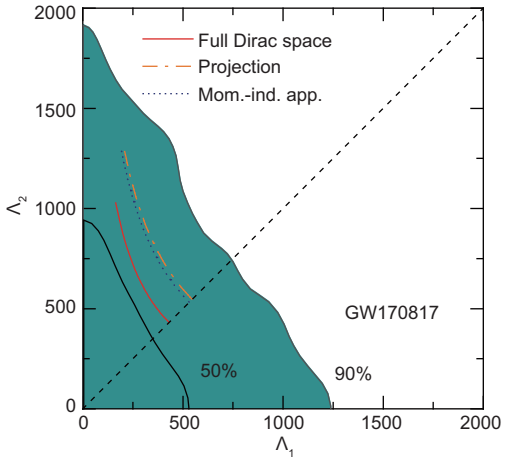

Figure 5 (Color online) Tidal deformabilities Λ_1 and Λ_2 associated with the high-mass M_1 and low-mass M_2 components of the binary neutron star obtained by the RBHF theory in the full Dirac space (red solid line), in comparison with the results obtained by the projection method (orange dash-dotted line) and the mom.-ind. app. method (blue dotted line). The diagonal dashed line denotes the boundary of $\Lambda_1 = \Lambda_2$. The 50% and 90% probability contours are extracted from GW170817 [5].

This work was supported by the National Natural Science Foundation of China (Grant Nos. 12205030, 12147102, and 12265012), Guizhou Provincial Science and Technology Projects (Grant No. ZK[2022]203), Construction Project of Characteristic Key Laboratory in Guizhou Colleges and Universities (Grant No. KY[2021]003), Key Laboratory of Guizhou Minzu University (Grant No. GZMUSYS[2021]03), Fundamental Research Funds for the Central Universities (Grant Nos. 2020CDJQY-Z003, and 2021CDJZYJH-003), and MOST-RIKEN Joint Project "Ab initio investigation in nuclear physics". Part of this work was achieved by using the supercomputer OCTOPUS at the Cybermedia Center, Osaka University under the support of the Research Center for Nuclear Physics of Osaka University.

1 B. A. Li, B. J. Cai, W. J. Xie, and N. B. Zhang, Universe **7**, 182 (2021), arXiv: 2105.04629.
2 D. Adhikari, et al. (PREX Collaboration), Phys. Rev. Lett. **126**, 172502 (2021), arXiv: 2102.10767.
3 D. Adhikari, et al. (CREX Collaboration), Phys. Rev. Lett. **129**, 042501 (2022), arXiv: 2205.11593.
4 J. M. Lattimer, Annu. Rev. Nucl. Part. Sci. **71**, 433 (2021).
5 B. P. Abbott, et al. (LIGO Scientific Collaboration, and Virgo Collaboration), Phys. Rev. Lett. **121**, 161101 (2018), arXiv: 1805.11581.
6 S. Gandolfi, A. Gezerlis, and J. Carlson, Annu. Rev. Nucl. Part. Sci. **65**, 303 (2015), arXiv: 1501.05675.
7 B. Alex Brown, Phys. Rev. Lett. **85**, 5296 (2000).
8 B. Y. Sun, W. H. Long, J. Meng, and U. Lombardo, Phys. Rev. C **78**, 065805 (2008), arXiv: 0910.4236.
9 Q. Zhao, Z. Ren, P. Zhao, and J. Meng, Phys. Rev. C **106**, 034315 (2022), arXiv: 2207.01764.
10 C. J. Jiang, Y. Qiang, D. W. Guan, Q. Z. Chai, C. Y. Qiao, and J. C. Pei, Chin. Phys. Lett. **38**, 052101 (2021), arXiv: 2012.14083.
11 J. Liu, C. Gao, N. Wan, and C. Xu, Nucl. Sci. Tech. **32**, 117 (2021).
12 A. Akmal, V. R. Pandharipande, and D. G. Ravenhall, Phys. Rev. C **58**, 1804 (1998), arXiv: nucl-th/9804027.
13 S. Gandolfi, A. Y. Illarionov, K. E. Schmidt, F. Pederiva, and S. Fantoni, Phys. Rev. C **79**, 054005 (2009), arXiv: 0903.2610.
14 K. Hebeler, S. K. Bogner, R. J. Furnstahl, A. Nogga, and A. Schwenk, Phys. Rev. C **83**, 031301 (2011), arXiv: 1012.3381.
15 G. Hagen, T. Papenbrock, A. Ekström, K. A. Wendt, G. Baardsen, S. Gandolfi, M. Hjorth-Jensen, and C. J. Horowitz, Phys. Rev. C **89**, 014319 (2014), arXiv: 1311.2925.

16 J. J. Lu, Z. H. Li, C. Y. Chen, M. Baldo, and H. J. Schulze, Phys. Rev. C **98**, 064322 (2018).
17 M. Baldo, and C. Maieron, Phys. Rev. C **69**, 014301 (2004), arXiv: nucl-th/0311070.
18 I. Bombaci, A. Fabrocini, A. Polls, and I. Vidaña, Phys. Lett. B **609**, 232 (2005), arXiv: nucl-th/0411057.
19 M. Baldo, A. Polls, A. Rios, H. J. Schulze, and I. Vidaña, Phys. Rev. C **86**, 064001 (2012), arXiv: 1207.6314.
20 M. Piarulli, I. Bombaci, D. Logoteta, A. Lovato, and R. B. Wiringa, Phys. Rev. C **101**, 045801 (2020), arXiv: 1908.04426.
21 A. Lovato, I. Bombaci, D. Logoteta, M. Piarulli, and R. B. Wiringa, Phys. Rev. C **105**, 055808 (2022), arXiv: 2202.10293.
22 W. Zuo, A. Lejeune, U. Lombardo, and J. F. Mathiot, Nucl. Phys. A **706**, 418 (2002).
23 G. E. Brown, W. Weise, G. Baym, and J. Speth, Comments Nucl. Part. Phys. **17**, 39 (1987).
24 F. Sammarruca, B. Chen, L. Coraggio, N. Itaco, and R. Machleidt, Phys. Rev. C **86**, 054317 (2012), arXiv: 1209.5001.
25 S. Shen, H. Liang, W. H. Long, J. Meng, and P. Ring, Prog. Part. Nucl. Phys. **109**, 103713 (2019), arXiv: 1904.04977.
26 B. D. Day, Rev. Mod. Phys. **39**, 719 (1967).
27 M. Baldo, and C. Maieron, J. Phys. G-Nucl. Part. Phys. **34**, R243 (2007).
28 R. Brockmann, and R. Machleidt, Phys. Rev. C **42**, 1965 (1990).
29 G. Q. Li, R. Machleidt, and R. Brockmann, Phys. Rev. C **45**, 2782 (1992).
30 D. Alonso, and F. Sammarruca, Phys. Rev. C **67**, 054301 (2003), arXiv: nucl-th/0301032.
31 H. Tong, X. L. Ren, P. Ring, S. H. Shen, S. B. Wang, and J. Meng, Phys. Rev. C **98**, 054302 (2018), arXiv: 1808.09138.
32 C. Wang, J. Hu, Y. Zhang, and H. Shen, J. Phys. G-Nucl. Part. Phys. **47**, 105108 (2020), arXiv: 2007.01726.
33 C. J. Horowitz, and B. D. Serot, Nucl. Phys. A **464**, 613 (1987).
34 L. Sehn, C. Fuchs, and A. Faessler, Phys. Rev. C **56**, 216 (1997), arXiv: nucl-th/9701060.
35 C. Fuchs, T. Waindzoch, A. Faessler, and D. S. Kosov, Phys. Rev. C **58**, 2022 (1998), arXiv: nucl-th/9709072.
36 T. Gross-Boelting, C. Fuchs, and A. Faessler, Nucl. Phys. A **648**, 105 (1999).
37 E. N. E. van Dalen, C. Fuchs, and A. Faessler, Nucl. Phys. A **744**, 227 (2004), arXiv: nucl-th/0407070.
38 E. N. E. van Dalen, C. Fuchs, C. Fuchs, and C. Fuchs, Eur. Phys. J. A **31**, 29 (2007), arXiv: nucl-th/0612066.
39 S. Wang, Q. Zhao, P. Ring, and J. Meng, Phys. Rev. C **103**, 054319 (2021), arXiv: 2103.12960.
40 S. Wang, H. Tong, and C. Wang, Phys. Rev. C **105**, 054309 (2022).
41 S. Wang, H. Tong, Q. Zhao, C. Wang, P. Ring, and J. Meng, Phys. Rev. C **106**, L021305 (2022), arXiv: 2203.05397.
42 H. Tong, C. Wang, and S. Wang, Astrophys. J. **930**, 137 (2022), arXiv: 2210.15241.
43 B. D. Serot, and J. D. Walecka, Adv. Nucl. Phys. **16**, 1 (1986).
44 M. R. Anastasio, L. S. Celenza, and C. M. Shakin, Phys. Rev. C **23**, 2273 (1981).
45 P. Poschenrieder, and M. K. Weigel, Phys. Rev. C **38**, 471 (1988).
46 R. H. Thompson, Phys. Rev. D **1**, 110 (1970).
47 J. X. Lu, C. X. Wang, Y. Xiao, L. S. Geng, J. Meng, and P. Ring, Phys. Rev. Lett. **128**, 142002 (2022), arXiv: 2111.07766.
48 R. Machleidt, Adv. Nucl. Phys. **19**, 189 (1989).
49 H. Shen, Y. Sugahara, and H. Toki, Phys. Rev. C **55**, 1211 (1997).
50 S. Ulrych, and H. Müther, Phys. Rev. C **56**, 1788 (1997), arXiv: nucl-th/9706030.
51 P. Ring, Prog. Part. Nucl. Phys. **37**, 193 (1996).
52 P. G. Krastev, and F. Sammarruca, Phys. Rev. C **74**, 025808 (2006), arXiv: nucl-th/0601065.
53 D. Lonardoni, I. Tews, S. Gandolfi, and J. Carlson, Phys. Rev. Res. **2**, 022033 (2020), arXiv: 1912.09411.
54 J. W. Holt, and N. Kaiser, Phys. Rev. C **95**, 034326 (2017), arXiv: 1612.04309.
55 B. P. Abbott, et al. (LIGO Scientific Collaboration, and Virgo Collaboration), Phys. Rev. Lett. **119**, 161101 (2017), arXiv: 1710.05832.
56 A. Goldstein, P. Veres, E. Burns, M. S. Briggs, R. Hamburg, D. Kocevski, C. A. Wilson-Hodge, R. D. Preece, S. Poolakkil, O. J. Roberts, C. M. Hui, V. Connaughton, J. Racusin, A. von Kienlin, T. Dal Canton, N. Christensen, T. Littenberg, K. Siellez, L. Blackburn, J. Broida, E. Bissaldi, W. H. Cleveland, M. H. Gibby, M. M. Giles, R. M. Kippen, S. McBreen, J. McEnery, C. A. Meegan, W. S. Paciesas, and M. Stanbro, Astrophys. J. **848**, L14 (2017), arXiv: 1710.05446.
57 V. Savchenko, C. Ferrigno, E. Kuulkers, A. Bazzano, E. Bozzo, S. Brandt, J. Chenevez, T. J. L. Courvoisier, R. Diehl, A. Domingo, L. Hanlon, E. Jourdain, A. von Kienlin, P. Laurent, F. Lebrun, A. Lutovinov, A. Martin-Carrillo, S. Mereghetti, L. Natalucci, J. Rodi, J. P. Roques, R. Sunyaev, and P. Ubertini, Astrophys. J. **848**, L15 (2017), arXiv: 1710.05449.
58 M. Du, and L. Xu, Sci. China-Phys. Mech. Astron. **65**, 219811 (2022), arXiv: 2101.12371.
59 E. Annala, T. Gorda, A. Kurkela, and A. Vuorinen, Phys. Rev. Lett. **120**, 172703 (2018), arXiv: 1711.02644.
60 J. Antoniadis, P. C. C. Freire, N. Wex, T. M. Tauris, R. S. Lynch, M. H. van Kerkwijk, M. Kramer, C. Bassa, V. S. Dhillon, T. Driebe, J. W. T. Hessels, V. M. Kaspi, V. I. Kondratiev, N. Langer, T. R. Marsh, M. A. McLaughlin, T. T. Pennucci, S. M. Ransom, I. H. Stairs, J. van Leeuwen, J. P. W. Verbiest, and D. G. Whelan, Science **340**, 1233232 (2013), arXiv: 1304.6875.
61 S. Huth, P. T. H. Pang, I. Tews, T. Dietrich, A. Le Févre, A. Schwenk, W. Trautmann, K. Agarwal, M. Bulla, M. W. Coughlin, and C. Van Den Broeck, Nature **606**, 276 (2022), arXiv: 2107.06229.
62 S. Wang, C. Wang, and H. Tong, Phys. Rev. C **106**, 045804 (2022), arXiv: 2206.08579.
63 P. B. Demorest, T. Pennucci, S. M. Ransom, M. S. E. Roberts, and J. W. T. Hessels, Nature **467**, 1081 (2010), arXiv: 1010.5788.
64 E. Fonseca, T. T. Pennucci, J. A. Ellis, I. H. Stairs, D. J. Nice, S. M. Ransom, P. B. Demorest, Z. Arzoumanian, K. Crowter, T. Dolch, R. D. Ferdman, M. E. Gonzalez, G. Jones, M. L. Jones, M. T. Lam, L. Levin, M. A. McLaughlin, K. Stovall, J. K. Swiggum, and W. Zhu, Astrophys. J. **832**, 167 (2016), arXiv: 1603.00545.
65 H. T. Cromartie, E. Fonseca, S. M. Ransom, P. B. Demorest, Z. Arzoumanian, H. Blumer, P. R. Brook, M. E. DeCesar, T. Dolch, J. A. Ellis, R. D. Ferdman, E. C. Ferrara, N. Garver-Daniels, P. A. Gentile, M. L. Jones, M. T. Lam, D. R. Lorimer, R. S. Lynch, M. A. McLaughlin, C. Ng, D. J. Nice, T. T. Pennucci, R. Spiewak, I. H. Stairs, K. Stovall, J. K. Swiggum, and W. W. Zhu, Nat. Astron. **4**, 72 (2020), arXiv: 1904.06759.
66 E. Fonseca, H. T. Cromartie, T. T. Pennucci, P. S. Ray, A. Y. Kirichenko, S. M. Ransom, P. B. Demorest, I. H. Stairs, Z. Arzoumanian, L. Guillemot, A. Parthasarathy, M. Kerr, I. Cognard, P. T. Baker, H. Blumer, P. R. Brook, M. DeCesar, T. Dolch, F. A. Dong, E. C. Ferrara, W. Fiore, N. Garver-Daniels, D. C. Good, R. Jennings, M. L. Jones, V. M. Kaspi, M. T. Lam, D. R. Lorimer, J. Luo, A. McEwen, J. W. McKee, M. A. McLaughlin, N. McMann, B. W. Meyers, A. Naidu, C. Ng, D. J. Nice, N. Pol, H. A. Radovan, B. Shapiro-Albert, C. M. Tan, S. P. Tendulkar, J. K. Swiggum, H. M. Wahl, and W. W. Zhu, Astrophys. J. Lett. **915**, L12 (2021), arXiv: 2104.00880.
67 F. J. Fattoyev, J. Piekarewicz, and C. J. Horowitz, Phys. Rev. Lett. **120**, 172702 (2018), arXiv: 1711.06615.
68 I. Tews, J. Margueron, and S. Reddy, Phys. Rev. C **98**, 045804 (2018), arXiv: 1804.02783.
69 I. Tews, J. Margueron, and S. Reddy, Eur. Phys. J. A **55**, 97 (2019), arXiv: 1901.09874.
70 B. P. Abbott, et al. (LIGO Scientific Collaboration, and Virgo Collaboration), Phys. Rev. X **9**, 011001 (2019), arXiv: 1805.11579.